

Characterization of blue and yellow straggler stars of Berkeley 39 using *Swift*/UVOT

KOMAL CHAND ^{1,*} KHUSHBOO RAO ^{1,2,†} KAUSHAR VAIDYA,^{1,‡} AND ANJU PANTHI^{1,§}

¹*Department of physics, Birla Institute of Technology and Science-Pilani, 333031 Rajasthan, India.*

²*Institute of Astronomy, National Central University, 300 Zhongda Road, Zhongli 32001 Taoyuan, Taiwan.*

ABSTRACT

We characterize blue straggler stars (BSS) and yellow straggler stars (YSS) of an open cluster (OC) Berkeley 39 using multi-wavelength observations including *Swift*/UVOT. Our analysis also makes use of ultraviolet (UV) data from *GALEX*, optical data from *Gaia* DR3 and Pan-STARRS, and infrared data from 2MASS, *Spitzer*/IRAC, and *WISE*. Berkeley 39 is a ~ 6 Gyr old Galactic OC located at a distance of ~ 4200 pc. We identify 729 sources as cluster members utilizing a machine learning algorithm, ML-MOC, on *Gaia* DR3 data. Of these, 17 sources are classified as BSS candidates and four as YSS candidates. We construct multi-wavelength spectral energy distributions (SEDs) of 16 BSS and 2 YSS candidates, within the *Swift*/UVOT field, to analyze their properties. Out of these, 8 BSS candidates and both the YSS candidates are successfully fitted with single-component SEDs. Five BSS candidates show marginal excess in the near-UV (fractional residual < 0.3 in all but one UVOT filter), whereas three BSS candidates show moderate to significant excess in the near-UV (fractional residual > 0.3 in at least two UVOT filters). We present the properties of the BSS and YSS candidates, estimated based on the SED fits.

Keywords: ultraviolet: stars — (stars:) blue straggler stars — (stars:) colour magnitude diagrams — (stars:) open clusters and associations: individual: (Berkeley 39)

1. INTRODUCTION

Binary stars, ranging from close binaries to wide binaries, are common in star clusters. They play a significant role in star clusters, contributing to their dynamical and evolutionary processes. The interactions among close binary stars and multiple stellar systems can lead to intriguing, unique stellar populations in star clusters. Notable outcomes of such interactions are blue straggler stars (BSS, Sandage 1953), yellow straggler stars (YSS, Strom et al. 1971; Leiner et al. 2016), red straggler stars (Geller et al. 2017), cataclysmic variables (Ritter 2010), etc. BSS are located above the main sequence turn-off (MSTO) in the clusters' colour-magnitude diagrams (CMDs). This location on the CMDs indicates that they have higher temperatures and luminosities than the MSTO. BSS are observed in diverse stellar environments such as open clusters (OCs, Ahumada & Lapasset 2007; Jadhav et al. 2021; Rain et al. 2021), globular clusters (GCs, Sandage 1953; Nikitha et al. 2022), Galactic fields (Carney et al. 2005) and dwarf galaxies (Momany et al. 2007). Observational studies have shown that BSS are among the most massive members of star clusters (Shara et al. 1997; Gilliland et al. 1998; Fiorentino et al. 2014). Therefore, they are supposed to segregate towards the clusters' centers faster than any other cluster population. The radial distributions of BSS are used to categorize GCs and OCs in different dynamical ages (Ferraro et al. 2012; Vaidya et al. 2020; Rao et al. 2021, 2023). Thus, BSS provide valuable insights to probe the relationship between stellar evolution and stellar dynamics (Bailyn 1995). Although much rarer compared to the BSS, YSS are frequently found in CMDs as objects relatively redder than the BSS and brighter than the subgiants (Leiner et al. 2016). The first YSS was discovered in an OC M67 by Janes & Smith (1984). Landsman et al. (1997) studied this object, a yellow giant, S1040, using the Hubble Space Telescope, and found a white dwarf (WD) companion associated with it. Recently, Rain et al. (2021) have identified 77 potential YSS among 408 OCs using the *Gaia* DR2 data (Gaia Collaboration et al. 2018). Hot companions of few

* p20210463@pilani.bits-pilani.ac.in

† khushboo@gm.astro.ncu.edu.tw

‡ kaushar@pilani.bits-pilani.ac.in

§ p20190413@pilani.bits-pilani.ac.in

YSS have been identified in OCs, NGC 2506 (Panthi et al. 2022), NGC 6940 (Panthi & Vaidya 2024) and NGC 2627 (Saketh et al. 2024) using the *Astrosat*/UVIT (Agrawal 2017) data.

Formation mechanisms of BSS are still debatable and are an active field of research (Boffin et al. 2015). There are three widely accepted formation pathways of BSS, direct stellar collisions, mass transfer (MT) in a binary, and mergers. Direct stellar collisions may lead to formation of a single massive BSS (Hills & Day 1976; Leonard 1996). In hierarchical triple systems, components of the inner binary may have a MT or merger as a result of the Kozai mechanism, leading to the formation of a binary BSS or single massive BSS, respectively (Perets & Fabrycky 2009). MT efficiency can be conservative or non-conservative, depending on the orbital periods and mass ratio of a binary system (Leiner & Geller 2021). Observational evidence of BSS with WD companions in low-density environments such as OCs raised the possibility of MT as a possible pathway (Gosnell et al. 2015). Based on the evolutionary phase of the primary star, the MT process is further divided into three cases. In Case A, a compact binary system consisting of two main-sequence (MS) stars may undergo merger via stellar winds or a MT process, leaving behind a single massive BSS, or it may undergo MT via Roche lobe overflow, leaving behind a BSS with an MS companion (Vilhu 1982). In Case B, the MT occurs in a long-period binary system ($P \sim 1 - 1000$ days) when the primary is in the RGB phase, leaving behind a binary BSS with a He WD companion Landsman et al. (1997). Finally, in Case C, the MT occurs in a wide binary system ($P \sim 1000 - 2000$ days) when the primary is in the AGB phase, leaving behind a binary BSS with a Carbon-Oxygen (CO) WD companion (Gosnell et al. 2014). There is a fourth possible pathway of BSS formation via MT. In wide binary systems with periods ranging from $\sim 1000 - 10000$ days, MT may also occur via wind Roche lobe overflow (WRLOF, Geller & Mathieu 2011) when the primary is in the AGB phase (Case D), leaving behind a binary BSS with a CO WD companion. As mentioned above, various mechanisms contribute to BSS formation, and determining the precise pathway is challenging without details about their orbital parameters and companions. Multiple mechanisms have been found to be dominant in a given cluster (Ferraro & Lanzoni 2006; Mathieu et al. 2009). In low-density environments such as OCs and Galactic fields, MT and merger pathways are dominant, while high-density environments such as the cores of GCs may also form BSS via the collision pathway (Davies et al. 2004). YSS are considered the evolved BSS, i.e., the post MS stars more massive than the MSTO, on their way to becoming the RGB stars (Mathieu et al. 1990). Through an asteroseismic mass and radius measurements of a YSS S1237 in OC M67, Leiner et al. (2016) concluded that it has formed either due to stellar collision or binary merger.

Ultraviolet (UV) wavelengths are more suitable for studying exotic populations like BSS and YSS. Being hotter objects, they emit a significant fraction of their flux in the UV wavelengths. Moreover, binary BSS and YSS with a WD companion would show an excess flux in the UV, which may be used to characterize them. Stellar hot spots in contact and semi-detached binaries also enhance UV flux (Kouzuma 2019). Magnetic activity and chromospheric processes also contribute to the total UV flux emitted by single and binary stars of intermediate-age star clusters. Additionally, flares on the stars serve as a transient source of UV radiation and in X-rays (Dempsey et al. 1993; Mitra-Kraev et al. 2005). Hence, it is important to understand the source of UV excess flux in known binary systems, which could be due to the intrinsic property of the star or due to the presence of a hot companion. Gosnell et al. (2015) detected 4 hot WD companions and 3 cool WD companions (11,000 K – 12,000 K) for BSS of NGC 188 using Hubble Space Telescope (HST) observations in far-ultraviolet (FUV) filters. Similar work has been done for other OCs using *Astrosat*/UVIT observations (Subramaniam et al. 2016, 2018; Jadhav et al. 2021; Panthi et al. 2022; Vaidya et al. 2022; Panthi et al. 2024) as well as *Swift*/UVOT observations (Rao et al. 2022). Recently, Panthi & Vaidya (2024) also studied WD companions for other exotic populations, including YSS, blue lurkers (BLs), and red clump stars of NGC 6940 using *Astrosat*/UVIT data.

Berkeley 39 ($\alpha = 7^h 46^m 42^s$, $\delta = -4^h 36^m 00^s$) is a 6 Gyr (Kassisi et al. 1997) old OC having mass $\sim 2 \times 10^4 M_\odot$ and mean metallicity $[\text{Fe}/\text{H}] = -0.20$ (Bragaglia et al. 2012), located at a distance of 4200 pc (Vaidya et al. 2020). The BSS population of this cluster has been previously studied by Vaidya et al. (2020) and Rao et al. (2023) using the *Gaia* EDR3 data (Gaia Collaboration et al. 2021). Vaidya et al. (2020) identified 23 BSS whereas Rao et al. (2023) identified 17 BSS. They found this cluster to be dynamically young or intermediate age based on the segregation of its BSS with respect to other less massive reference populations. This cluster has been subjected to various photometric and spectroscopic studies (Bragaglia et al. 2012), along with the identification of BSS. However, it has never been studied using UV imaging observations. Characterization of two BSS of this cluster using multi-wavelength SEDs,

including the Swift/UVOT data, are presented in Chand et al. (2024). With an aim to characterize the BSS and YSS populations of this cluster using multi-wavelength spectral energy distributions (SEDs), we study this cluster. The paper is arranged as follows. In §2, we give information about the data used for the present work and membership determination of the cluster. In §3, we present the results obtained. Finally, in §4, we present the discussion and summary of the work.

2. DATA AND MEMBERSHIP IDENTIFICATION

In order to characterize the BSS and YSS populations, we use multiwavelength data, ranging from UV to infrared (IR). In the subsections below, we provide the details of the archival data from various surveys and the cluster membership determination using the machine learning-based membership algorithm, ML-MOC (Agarwal et al. 2021), on the *Gaia* DR3 data (Vallenari et al. 2023).

2.1. UV data

The fluxes of sources in UV wavelengths are obtained from the Ultraviolet and Optical Telescope (*Swift*/UVOT; Gehrels et al. 2004) and Galaxy Evolution Explorer (*GALEX*; Martin et al. 2005). *Swift* spacecraft is equipped with three main instruments, namely Burst Alert Telescope (BAT), sensitive in the energy range of 3.0 – 150.0 keV, X-ray Telescope (XRT), sensitive in the energy range of 0.3 – 10.0 keV, and UVOT, sensitive in the optical/UV band in the wavelength range of 170 – 650 nm. UVOT is a modified Ritchey-Chretien UV/optical telescope having a diameter of 30 cm and provides a wide-field view of $17' \times 17'$. This instrument utilizes various filters, including clear white filters, U (300 – 400 nm), B (380 – 500 nm), V (500 – 600 nm), UVW1 (220 – 400 nm), UVM2 (200 – 280 nm), and UVW2 (180 – 260 nm), two grisms, a magnifier and a blocked filter (Roming et al. 2005). We utilize near-UV (NUV) data (Siegel et al. 2019) from UVOT in this work. Berkeley 39 was observed by *Swift*/UVOT in three UV filters, UVW2, UVM2, and UVW1, in 2011. The details of observations, the total number of detections, and the ML-MOC (described in Section 2.4) counterparts of cluster members in all three filters are listed in Table 1. In addition to the *Swift*/UVOT data, we also use the *GALEX* data to study our targets. *GALEX* is a 50 cm aperture space-based telescope (Martin et al. 2005) that operates in two UV bands, FUV (1350 – 1780 Å) and NUV (1770 – 2730 Å). For Berkeley 39, fluxes are available in the NUV filter alone.

Table 1. Observation details of OC Berkeley 39 using *Swift*/UVOT

Filter	λ_{eff} (Å)	Exposure (seconds)	Detections	Counterparts (ML-MOC members)
UVW2	2085.73	522	178	40
UVM2	2245.78	637	243	35
UVW1	2684.14	592	519	166

2.2. Optical Data

Gaia data (Vallenari et al. 2023) provides proper motions, parallaxes, and three-band photometry (G, G_{BP} , G_{RP}) for over a billion sources. The wavelength of filter G is centred at 673 nm, G_{BP} at 532 nm, and G_{RP} at 797 nm (Jordi et al. 2010). The Panoramic Survey Telescope and Rapid Response System (Pan-STARRS; Schlafly et al. 2012) is a ground-based telescope. It utilises five filters, g, r, i, z, and y, with effective wavelengths 481, 617, 752, 866, and 962 nm (Tonry et al. 2012), respectively.

2.3. IR Data

Two Micron All Sky Survey (2MASS; Cohen et al. 2003) contains near-IR photometric measurements in the J (1.24 μm), H (1.66 μm), and K_s (2.16 μm) bands. *Spitzer*/IRAC is a space-based observatory containing a four-channel camera that provides mid-IR wavelength fluxes (Fazio et al. 2004). IRAC provides $5.2' \times 5.2'$ simultaneous broadband images at I1 (3.6 μm), I2 (4.5 μm), I3 (5.8 μm), and I4 (8.0 μm). In 2006, *spitzer*/IRAC observed Berkeley 39 in all four IRAC channels with an exposure time of 26.8 s. Fazio et al. (2004) provides information about sources detected in all four filters, I1, I2, I3, and I4. Wide-field Infrared Survey Explorer (*WISE*; Wright et al. 2010) is a mid-IR full sky survey. It includes a 40 cm diameter telescope and four infrared detectors, namely, W1, W2, W3, and W4, with

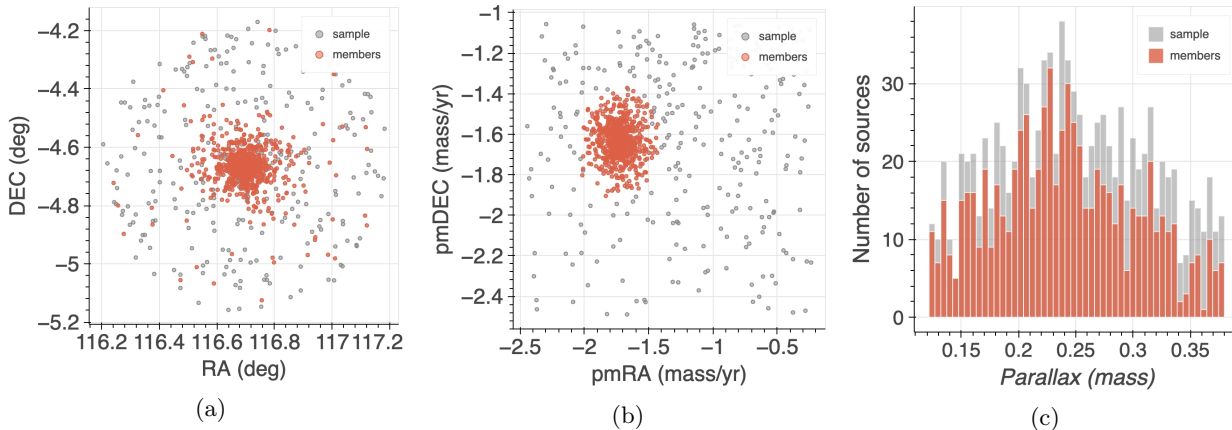


Figure 1. (a) The spatial distribution (b) proper motion distribution and (c) parallax distribution using ML-MOC algorithm on *Gaia* DR3 data.

wavelengths centred at $3.35 \mu\text{m}$, $4.60 \mu\text{m}$, $11.56 \mu\text{m}$, and $22.09 \mu\text{m}$, respectively. Since the *Spitzer*/IRAC filters have better resolution than WISE, we use WISE W1, W2 fluxes only when *Spitzer*/IRAC fluxes are unavailable.

2.4. Membership Identification

We use a machine-learning based membership determination algorithm, ML-MOC, for determination of cluster members (Agarwal et al. 2021). ML-MOC uses parallax and proper motion from *Gaia* data to identify cluster members and does not require prior knowledge about the cluster. It is based on the k-Nearest Neighbour (kNN, Cover & Hart 1967) and the Gaussian mixture model (GMM, Peel & McLachlan 2000) algorithms. The steps followed to determine the cluster members are summarised as follows. Initially, we download sources within $30'$ radius from the cluster center. These sources are required to have five astrometric parameters (RA, DEC, pmRA, pmDEC, and parallax), appropriate measurements in the *Gaia* photometric passbands (G, G_{BP} , and G_{RP}), non-negative parallaxes, and G-magnitude errors less than 0.005 mag. This group of sources is denoted as *All sources*. Subsequently, we employ kNN algorithm to eliminate probable field stars and determine *Sample sources* with a higher fraction of cluster members. Then, we apply the GMM to the *Sample sources* to separate the likely cluster members from the field stars. The GMM also provides the membership probabilities for each source. First, we select high-probability members with membership probabilities greater than 0.6, and then we include sources with membership probabilities between 0.2 and 0.6 to obtain the complete catalog of the cluster. For further details on the ML-MOC algorithm, readers are referred to Agarwal et al. (2021). We obtained 659 sources with cluster membership probabilities ≥ 0.6 and additional 70 sources with probabilities between 0.2 and 0.6. By plotting the radial distribution of identified cluster members, we estimated the cluster radius to be $14'$. The cluster radius estimated by us is in agreement with that estimated by Rao et al. (2023). Figure 1 shows the spatial, proper motion, and parallax distribution of sample sources and cluster members of Berkeley 39.

3. RESULTS

3.1. The Colour Magnitude Diagram

Figure 2a shows the spatial distribution of cluster members within $14'$ radius, with the BSS and YSS marked on the figure. The optical CMD for cluster members obtained using ML-MOC algorithm on *Gaia* DR3 data is shown in Figure 2b. Additionally, a PARSEC isochrone (Bressan et al. 2012) is overlaid on the CMD using the known age, 6 Gyr (Kassis et al. 1997) and metallicity, $[\text{Fe}/\text{H}] = -0.20$ from Bragaglia et al. (2012). For distance, extinction, A_G , and reddening, $E(\text{BP}-\text{RP})$, mean distance for bright ($G < 16$ mag) members using Bailer-Jones et al. (2021), and median values of the A_G and $E(\text{BP}-\text{RP})$ were used. To fit the isochrone, some fine-tuning of parameters was necessary. The final parameters of the isochrone are an age of 6 Gyr, distance of 4200 parsec, extinction, A_G , of 0.41 mag, and color-excess $E(\text{BP}-\text{RP})$, of 0.16 mag. The fundamental parameters used here to plot isochrone are consistent with those in Rao et al. (2023). Among the 729 cluster members, 17 stars are identified as BSS candidates. Additionally, 4 cluster members are found to lie between the region occupied by the BSS and the RGB. These are identified as the YSS candidates. The magnitudes of the BSS candidates range from 0 – 2 magnitudes brighter as compared to the

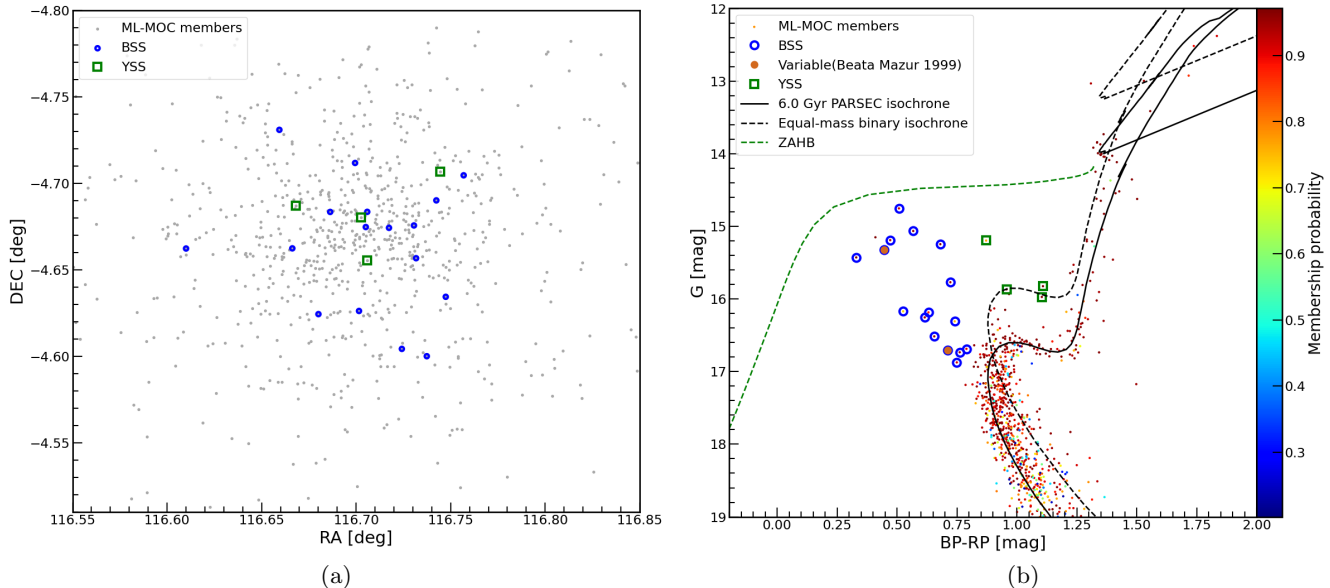


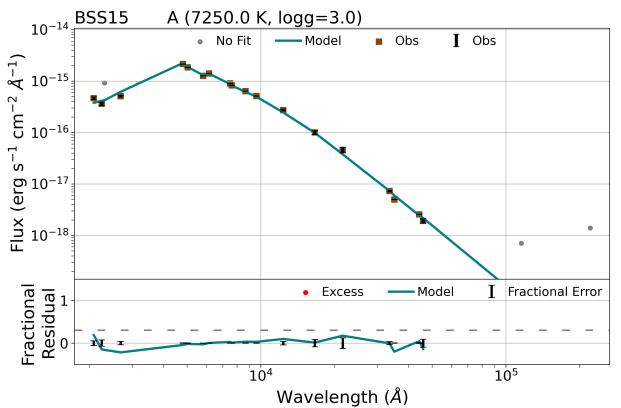
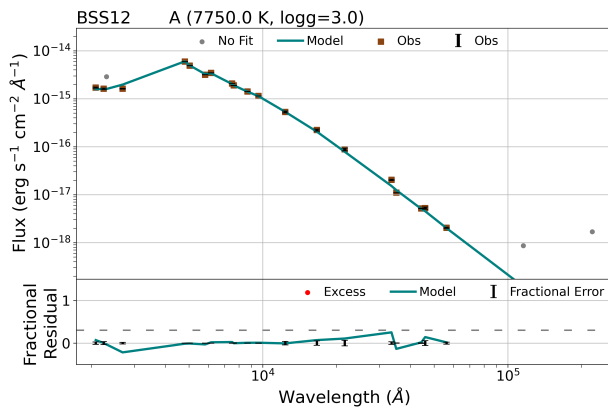
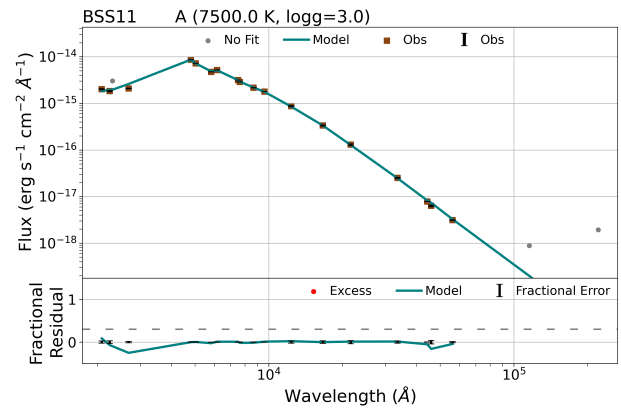
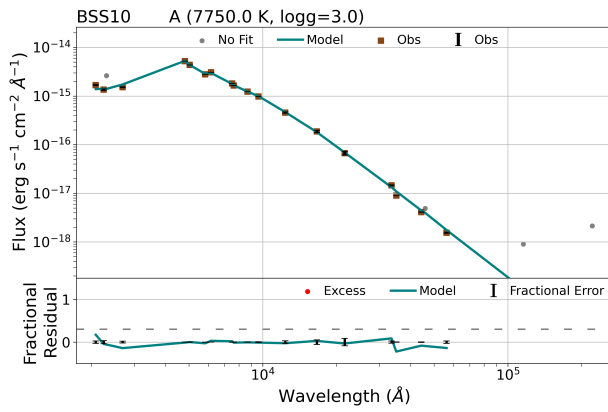
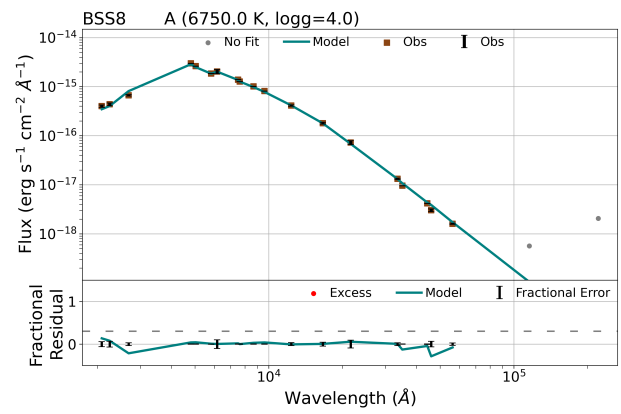
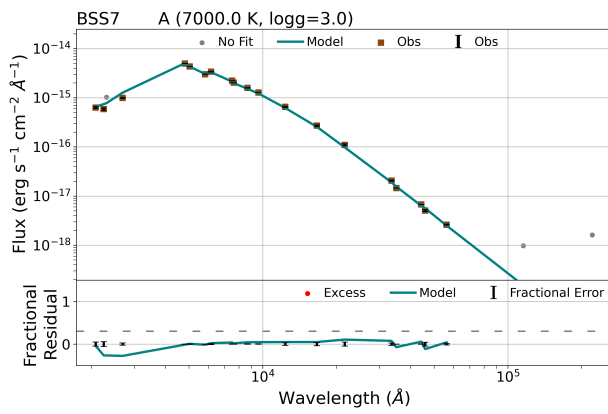
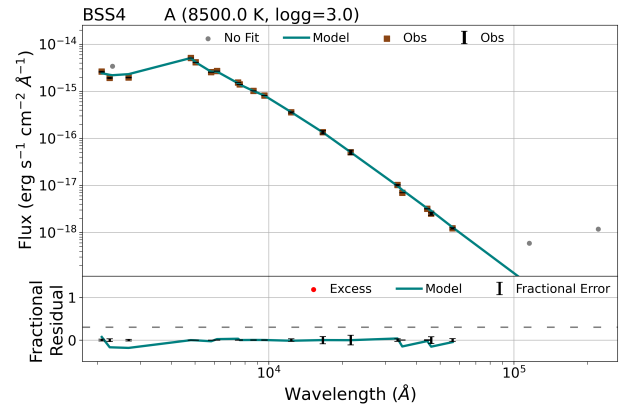
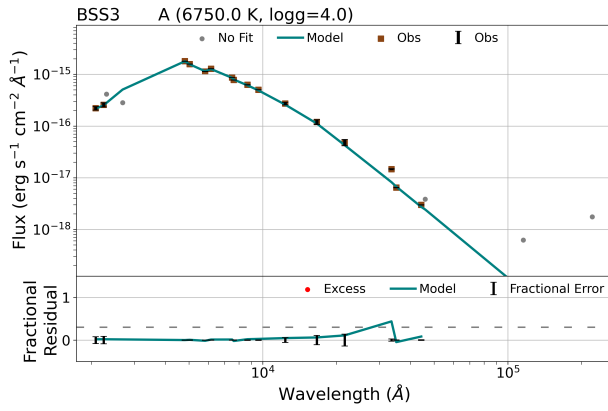
Figure 2. (a) Spatial distribution of the cluster members as grey data points, BSS marked with blue open circles and YSS marked with green open squares. (b) Optical CMD of cluster members of Berkeley 39 identified using the ML-MOC algorithm on *Gaia* DR3 members. The cluster members, along with their probabilities, are shown with auxiliary colours. The BSS and YSS are represented by blue open circles and green open squares, respectively. A PARSEC isochrone (Bressan et al. 2012) of age = 6 Gyr, distance = 4200 pc, extinction, $A_G = 0.41$ mag, and color-excess $E(BP-RP) = 0.16$ mag is overplotted on the CMD. The ZAHB is shown as a green dashed line and black dashed line shows equal-mass binary isochrone.

MSTO. As seen in the Figure 2, BSS candidates appear in two separate groups ($15.2 \text{ mag} < G < 16.8 \text{ mag}$) and ($16.2 \text{ mag} < G < 17 \text{ mag}$). However, all BSS candidates are seen well below the horizontal branch, and hence, we consider them to be the BSS candidates.

Out of these 17 BSS candidates and 4 YSS candidates, one BSS candidate and one YSS candidate lie outside the field of view of *Swift/UVOT*. For one YSS candidate, UV data is available only in one UVOT filter. Hence, we include 16 BSS candidates and 2 YSS candidates in our analysis. Of these, 5 BSS candidates and one YSS candidate are detected in three filters of *Spitzer/IRAC* (I1, I2, and I3), 10 BSS candidates are detected in at least two IRAC bands, and one BSS candidate and one YSS candidate are not detected in any of the *Spitzer/IRAC* filters. We use the data from WISE W1 and W2 bands for objects when *Spitzer/IRAC* data are not available. Furthermore two BSS, BSS6 and BSS10, are identified as variables by Mazur et al. (1999), shown as brown filled circles in the CMD. BSS6 has been identified as a possible eclipsing binary, whereas BSS10 has been identified as a δ -Scuti variable. *Gaia* DR3 lists them as variables; however, their variable nature is not identified. We searched for their TESS data, but they are not observed via TESS.

3.2. Spectral Energy Distributions

Multi-wavelength SEDs have been a vital tool in characterizing exotic stellar populations such as BSS and YSS. To estimate the fundamental parameters such as temperatures, radii, and luminosities of BSS and YSS candidates, we construct their multi-wavelength SEDs. Before we fit the SEDs, we utilize Aladin¹, a visualization tool, to examine any nearby sources within a $3''$ radial distance. None of the 16 BSS and 2 YSS candidates have a nearby source within $3''$; therefore, we construct their SEDs. The SEDs are constructed using the Virtual Observatory SED Analyzer (VOSA)². VOSA employs filter transmission curves to calculate synthetic photometry for a selected theoretical model. To generate SEDs, we provide distance to the cluster, 4200 pc, and extinction, A_V , 0.51 mag. The extinction, A_V , was derived from the median A_G of the cluster, using the correlation given in Wang & Chen (2019). VOSA collects fluxes in optical wavelength from *Gaia* DR3 and Pan-STARRS, near IR from 2MASS, and mid-IR data from *WISE*. We use the *WISE* W1 and W2 band fluxes for sources that do not have IRAC magnitudes in the I1 and I2 channels since the resolution of WISE is poorer compared to that of the IRAC. When only upper limits are available in any filters, they are not included in the fitting of the SEDs. VOSA corrects all of the observed fluxes for extinction using the extinction law given by Fitzpatrick (1999) and Indebetouw et al. (2005). To fit SEDs, we use Kurucz (Castelli et al.



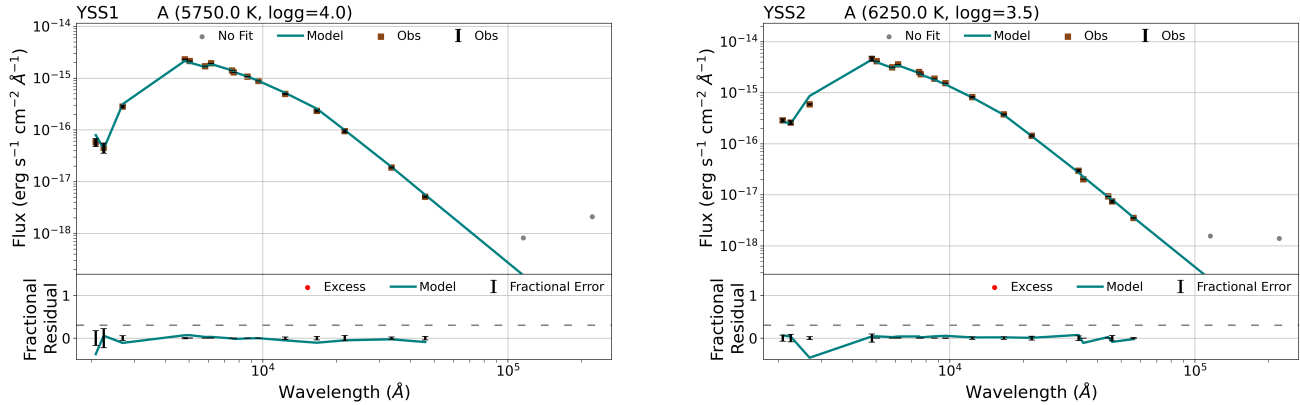


Figure 3. The single-component SED fits of BSS and YSS candidates. The top panels in each figure show extinction corrected observed fluxes in brown data points, with black error bars representing the errors in observed fluxes, and the blue curve representing the Kurucz stellar model fit. The bottom panels depict the residual between extinction-corrected observed fluxes and the model fluxes across the filters from UV to IR wavelengths. The grey data points are not included in the fitting. The dashed line in the lower panel represents a fractional residual of 0.3.

1997) stellar model. To ensure the reliability of SED fitting and to check the true flux of sources at UV wavelengths, we first exclude UV data points and fit the SEDs from optical to IR wavelength. VOSA suggests the best-fit SEDs based on the reduced χ^2 minimization. The value of χ^2 is calculated using the following formula:

$$\chi_r^2 = \frac{1}{N - N_f} \sum_{i=1}^N \frac{(F_{o,i} - M_d F_{m,i})^2}{\sigma_{o,i}^2} \quad (1)$$

Where N is the total number of photometric data points, N_f indicates the total number of fitted model parameters, $F_{o,i}$ is the observed flux, $F_{m,i}$ is the model flux of the star, $\sigma_{o,i}$ is the error in observed flux, and $M_d = (R/D)^2$ is the scaling factor, dependent on the radius and the distance of objects. The spatial coordinates, *Gaia* IDs, and *Swift*/*UVOT* fluxes, along with their errors, are listed in Table 2.

Figure 3 shows the SEDs of 8 BSS and 2 YSS candidates successfully fitted with a single temperature. The residual of the fits is nearly zero, implying that the model fits well to the observed fluxes. Our criteria for considering sources for a double-component fit is a fractional residual greater than 0.3 in at least two UVOT filters. In the Table 3, we list the value of fractional residual for all the three UVOT filters for all the BSS and YSS candidates. Five BSS candidates show lower fractional residuals, less than 0.3, in all but one UVOT filter. We do not consider them for the double fit. The SEDs of these five BSS are shown in Figure 4. As can be seen almost of all of them show an excess in the UVW2 filter which is the shortest wavelength among the three UV filters. There are three BSS candidates that exhibit fractional residuals exceeding 0.3 in at least two UVOT filters, thereby qualifying our criteria for a double-component SED fit. Such large UV excess could be due to the presence of a hot companion, chromospheric activity like hot spots in contact and semi-detached binaries, coronal emissions at very high temperatures, sub-luminous companions, magnetic activities of stars, flares on the stars, or active binaries. To understand the reason for the UV excess, we first searched for the X-ray counterparts of these sources. However, no X-ray data are available in *Chandra* or *XMM* for this cluster. In order to check the possibility of UV excess coming from an unresolved hot companion, we try to fit a double component SED using Koester (Koester 2010) and Kurucz (Castelli et al. 1997) model. In case of two BSS, BSS13 and BSS14, we are unable to fit the observed UV excess using the two-component SEDs as the model suggests an upper limit of temperature, ~ 80000 K, for the hot components. Hence, these two component fits are unreliable. The single-component SED fits of these three BSS with fractional residual greater than 0.3 are shown in Figure 5. As can be seen, for BSS13, the excess is detected in two UVOT filters, UVW1 and UVM2, whereas for BSS14, the excess is detected in all the three UVOT filters, UVW1, UVM2 and UVW2, as well as the *GALEX* NUV datapoint. The third BSS with fractional UV excess greater than 0.3 in at least two UVOT filters, BSS16, is successfully fitted

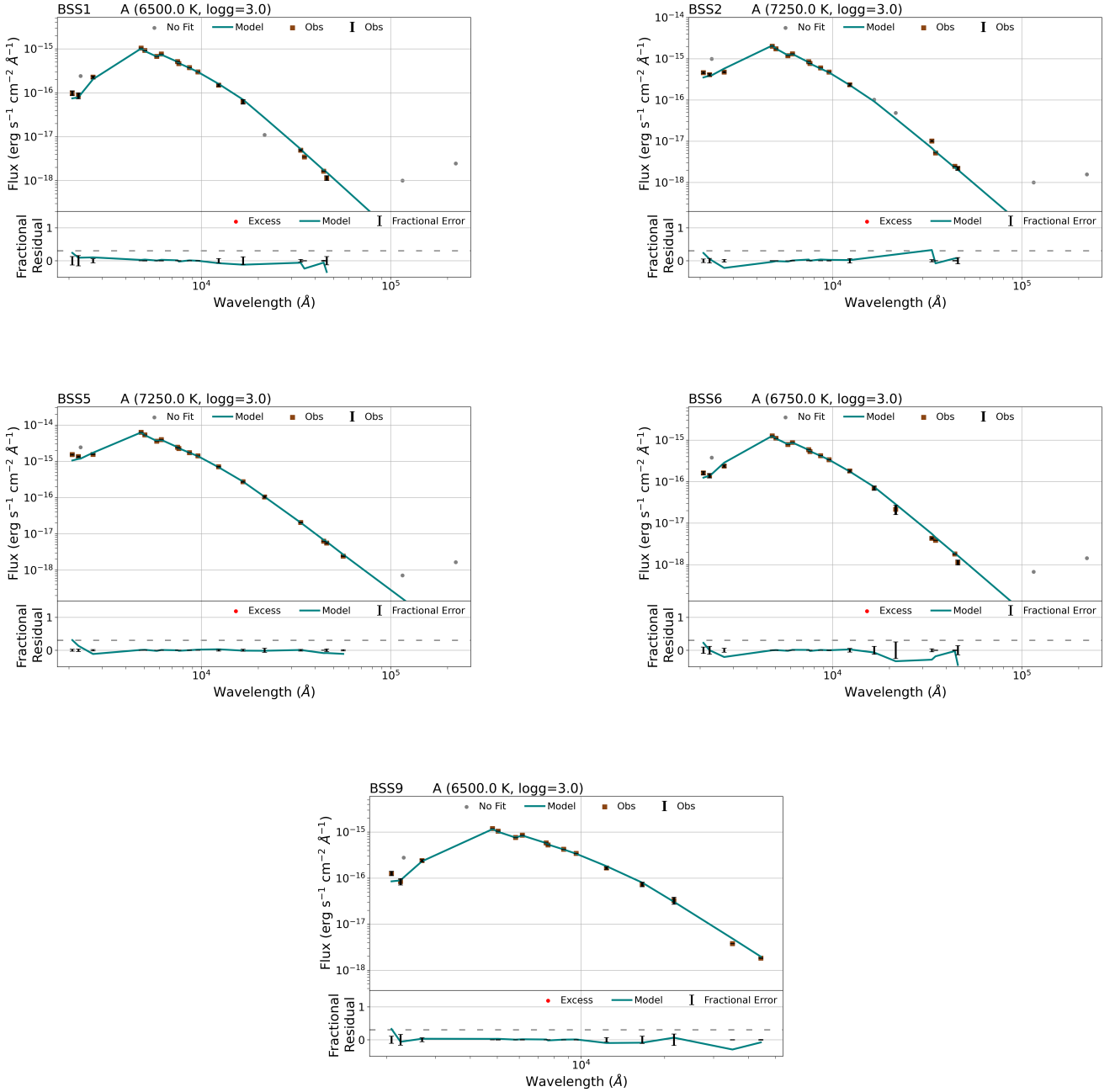


Figure 4. The single-component SED fits of BSS having fractional residual less than 0.3 in all but in one UVOT filter. The symbols and curves mean the same as in Figure 3.

with a double-component SED. We fit the hot component with the Koester model (Koester 2010) whereas the cool component is fitted with the Kurucz model (Castelli et al. 1997). Based on the SED fit (see Figure 6), we estimate that the hot component has a temperature of 12500 ± 125 K, a radius of $0.05 \pm 0.01 R_{\odot}$, and a luminosity of $0.06 \pm 0.02 L_{\odot}$. The parameters of all BSS, YSS, and their companion obtained from SED fits are listed in Table 3.

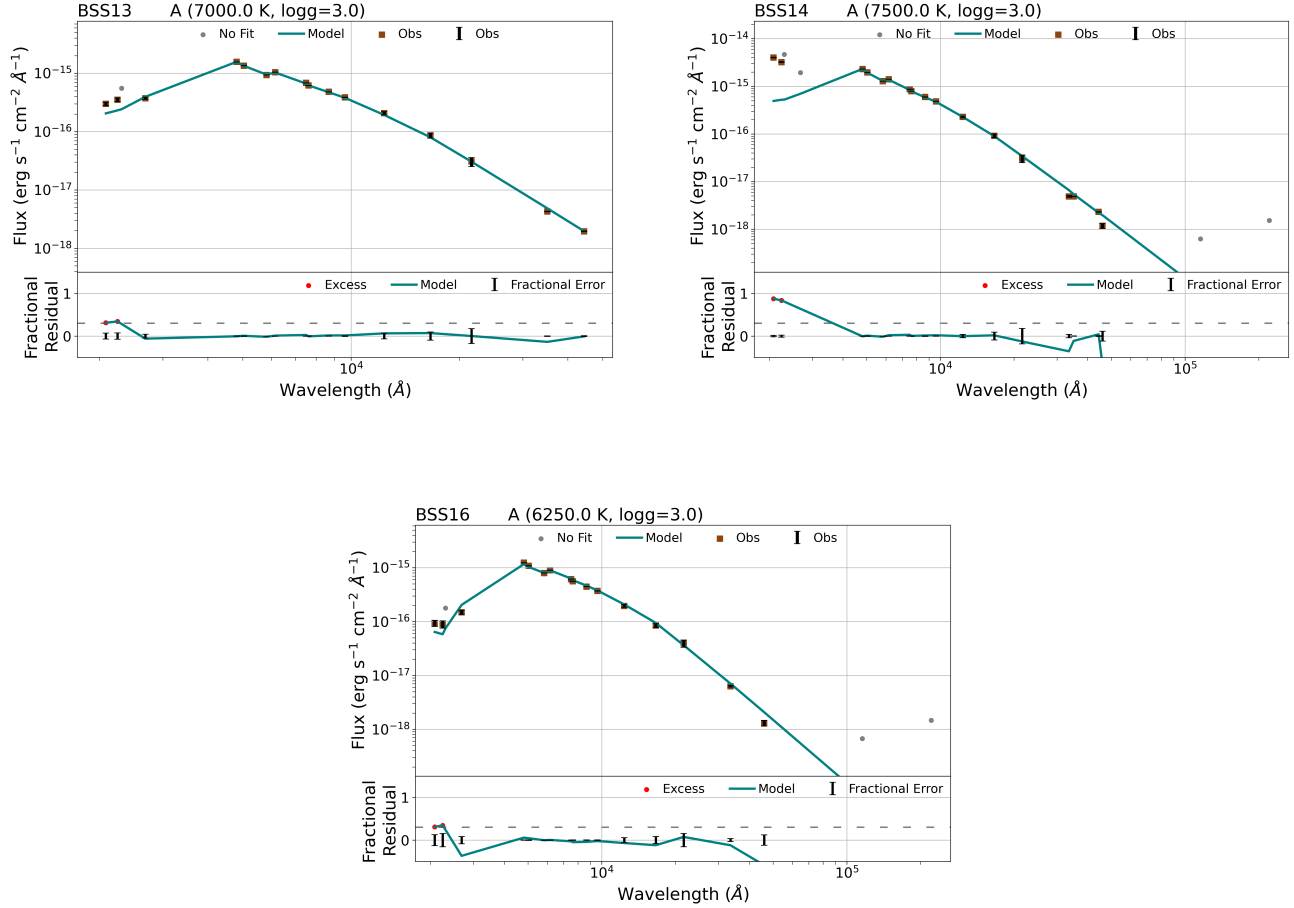


Figure 5. The single component SED fit of BSS having fractional residual greater than 0.3 in at least two UVOT filters. The symbols and curves mean the same as in Figure 3.

4. DISCUSSION AND SUMMARY

The availability of data from *Swift*/UVOT for OC Berkeley 39 enabled us to study the exotic stars of this cluster in the NUV regime. To characterize BSS and YSS candidates of OC Berkeley 39, we utilized *Swift*/UVOT data in three filters: UVW2, UVM2, and UVW1, along with the other multi-wavelength data. We first identified the cluster members using a machine-learning algorithm, ML-MOC, on *Gaia* DR3 and obtained a total of 729 members, including 17 BSS and 4 YSS candidates. Out of the identified BSS and YSS candidates, we could study 16 BSS candidates and 2 YSS candidates since one BSS candidate and one YSS candidate lie outside the FOV of *Swift*/UVOT, whereas one YSS candidate is detected only in one of the UVOT filters. To estimate the fundamental parameters (temperatures, radii, and luminosities) of BSS and YSS candidates, we constructed multi-wavelength SEDs using a virtual observatory tool, VOSA. Apart from obtaining the fundamental parameters of the exotic stars, our objective was to search for the presence of unresolved hot companions in these stars. Similar studies have been previously carried out to investigate exotic populations of OCs using HST by Geller & Mathieu (2011); Gosnell et al. (2014), and Gosnell et al. (2015), *Astrosat*/UVIT by Subramaniam et al. (2016); Sindhu et al. (2019); Jadhav et al. (2019); Panthi et al. (2022); Vaidya et al. (2022); Panthi & Vaidya (2024); Panthi et al. (2024) and *Swift*/UVOT by Rao et al. (2022).

Of the identified BSS and YSS candidates in *Swift*/UVOT, 8 BSS and 2 YSS candidates fitted successfully with single-component SED. For these BSS, temperatures range from 6750 K to 8500 K, which is consistent given the age of the cluster, as also witnessed in a similar age OC M67 whose BSS have temperatures range from 6250 K – 9000 K

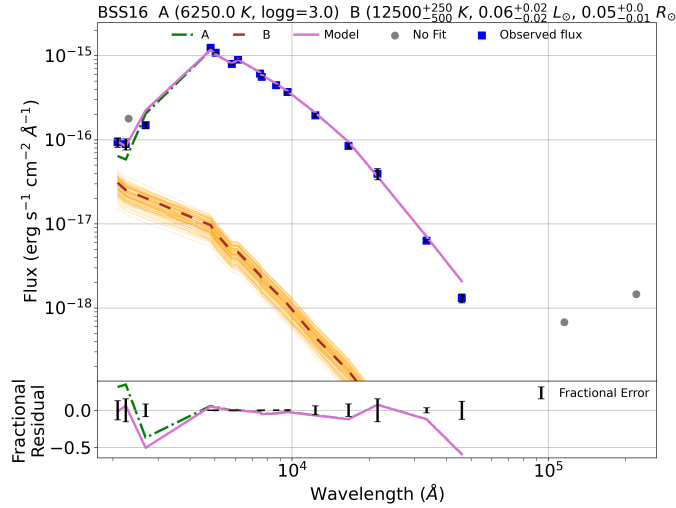


Figure 6. The binary-component SED of BSS16. The top panel displays the double component SED of each object, with blue data points representing extinction corrected flux values (labeled as “Observed flux”) and black error bars showing flux errors. The green dashed line represents the cool component fit (labeled as “A”), while the brown dashed line represents the hot (B) component fit (labeled as “B”), with orange curves representing iteration residuals. The composite fit is depicted as a pink curve (labeled as “Model”), with grey data points denoting data points that were not included in the fits (labeled as “No fit”). The fractional residual for single (green) and composite (pink) fits is shown in the bottom panel. On the x-axis, black error bars represent fractional errors (labeled as “Fractional error”). The cool and hot component parameters derived from the SED, as well as the estimated errors, are listed at the top of the plots.

(Sindhu et al. 2019). The luminosities for these eight BSS vary from $3.12 L_{\odot}$ to $12.89 L_{\odot}$. For YSS, the temperatures range from 5750 K to 6250 K, and luminosities vary from $7.03 L_{\odot}$ to $12.91 L_{\odot}$. The lower temperature range of YSS suggests that YSS are cooler as compared to BSS, which is expected since YSS are believed to be evolved BSS (Leiner et al. 2016). On the H-R diagram, shown in Figure 7, most of these eight BSS (open triangles), including BSS10 which is a δ -Scuti variable (Mazur et al. 1999), lie farther from the MSTO. Based on the extension of a single stellar isochrone of the cluster, their estimated mass gain ranges from $0.23 M_{\odot}$ to $0.56 M_{\odot}$ corresponding to a MSTO mass of $1.05 M_{\odot}$. The absence of UV-excesses in their CMDs, as well as their locations on the H-R diagram (farther from the MSTO) suggest that they may have formed via mergers. However, it is also possible that some of them have formed through MT, but their companion WDs are currently cooler than ~ 11000 K and therefore remain undetected.

Five BSS, including BSS6, which is likely an eclipsing binary (Mazur et al. 1999), show small amount of UV excess; fractional residual up to 0.3 in UVW2 filter. Since an excess in a single UV filter does not provide us an opportunity to obtain a reliable fit, we fit them with single-component SEDs here. These excesses could be due to presence of hot spots or chromospheric activity, or even the presence of a hot companion. It is worth noting that the excess is visible in the UVW2 filter, which is the shortest wavelength among the three NUV filters. Therefore, it is likely that the observed excess in these SEDs increases in the far UV wavelengths. However, the far UV data for this cluster are not available at the moment. As per the single-component fits, their temperatures range from 6500 K to 7250 K. Four of the five BSS are located closer to the MSTO on the H-R diagram (open circles). Assuming the single stellar isochrone, they seem to have gained mass from $0.15 M_{\odot}$ to $0.25 M_{\odot}$ with the exception of BSS5, which shows a larger mass gain of $0.54 M_{\odot}$. These smaller mass gains are consistent with MT by the Case-C formation mechanism (Chen & Han 2008). Therefore, the reason for the UV excess in a single filter is likely due to a hot companion, and these BSS may have formed via MT. However, for confirmation, far-UV data and/or spectroscopic observations are needed.

Objects that show moderate UV excess, fractional residual greater than 0.3 in at least two UV filters, are considered for double component SED fits. Three BSS meet this criterion, and we consider them for double component SED fits. The reasons for these UV excesses need to be looked into in further detail as the fractional residuals of 0.3 in at least two UV data points cannot be explained without either the presence of a WD companion or some other mechanisms, such as hot spots or chromospheric activities. The three BSS, BSS13, BSS14, and BSS16, have $T_{\text{eff}} \sim 6250$ K – 7500

K and L $\sim 2.12 L_{\odot} - 3.46 L_{\odot}$ based on single-component SEDs. To examine the possible reasons for UV excess in these three BSS, we searched for X-ray data in the *XMM* and *Chandra* catalogues, but the data are not available for this cluster. We tried to fit a double SED component using the binary-component SED fitting code (Jadhav et al. 2021) with Koester and Kurucz models. BSS16, having fractional residual greater than 0.3 in two of the UVOT filters, UVW2 and UVM2, fitted well with the Koester model corresponding to a hot component having a temperature, 12500^{+250}_{-500} K, a radius, $0.05 \pm 0.01 R_{\odot}$, and a luminosity, $0.06 \pm 0.02 L_{\odot}$. As can be seen in the H-R diagram (Figure 7), the hot companion of BSS16 lies very close to the WD cooling curve of $0.186 M_{\odot}$ (Panei et al. 2007), indicating it to be an ELM WD, assuming the UV excess is indeed due to the presence of a hot companion. Since ELM WDs cannot form through single star evolution within the age of the universe (Brown et al. 2011), this suggests that the progenitor of this WD must have undergone significant mass loss during its evolutionary process, supporting the Case A/Case B MT formation mechanism of BSS16. From the cooling age of the ELM WD as shown in Figure 7b, we can infer that the MT in this system ended recently, about 6.3 Myr ago. The primary component of BSS16 lies very close to and slightly below the MSTO in the H-R diagram, suggesting that this source could be called a BL.

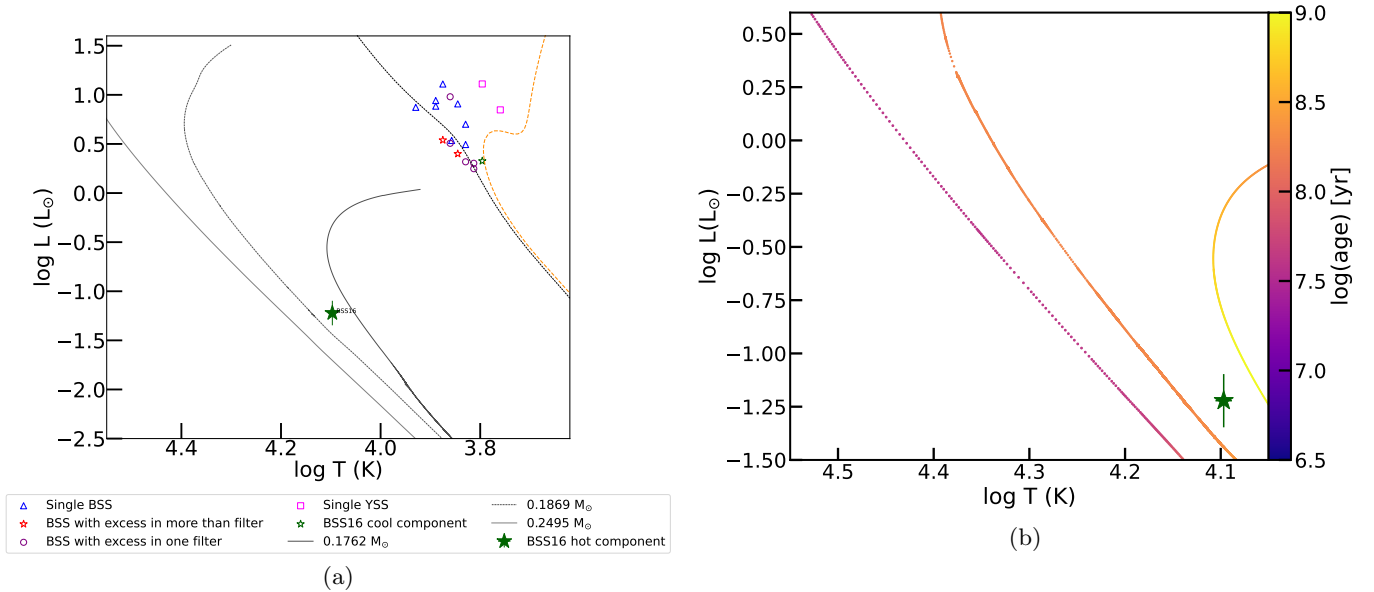


Figure 7. (a) H-R diagram showing the single-component BSS as blue open triangles and YSS as pink open squares. BSS with excess in more than one filter are shown as stars whereas BSS with excess in one filter is shown as open circles. The cooler component of BSS16 (most probably a BL or just a binary star) is shown with a green open star, and the hot companion associated with it is shown in a green solid star. An orange dotted curve represents a 6 Gyr PARSEC isochrone, and the ZAMS is depicted as a black dashed curve. Various solid grey curves represent low mass (LM) and ELM WD cooling curves of different masses, sourced from Panei et al. (2007) and Althaus et al. (2013). (b) The hot companion of BSS16 (most probably a BL or just a binary star) lies near the ELM WD cooling curves of $0.186 M_{\odot}$ (Panei et al. 2007), indicating its approximate cooling age.

For BSS13 and BSS14, the best-fitted double-component models reached the upper limit of the temperature for the hot component. Similar cases have been observed in other star clusters. In NGC 6940, one BL and one red clump star exhibited UV excess but could not be fitted with binary-component SEDs (Panthi & Vaidya 2024). Authors speculated that these two stars could be binary systems, and additional spectroscopic observations are needed to confirm. Alternatively, the UV excess may be due to other physical reasons such as hot spots, magnetic or chromospheric activities, or flares in a single or binary system. We need high-resolution spectroscopic observations to understand the reason for the UV excess in this system. The cool components of these two BSS are also lying near the MSTO suggesting a mass gain of less than $0.12 M_{\odot}$, indicating their origin is MT in a binary if the UV excess is not originated due to chromospheric activity or hot excess.

To conclude, of the 16 BSS whose SEDs are presented here, we speculate that eight may have formed via mergers or MT with companion WDs cooler than ~ 11000 K whereas the remaining eight may have formed via MT. Of these eight

BSS that likely originated in MT, we are able to characterize the hot companion of a single BSS, BSS16. Based on the properties of this hot companion, it appears to be an ELM WD, suggesting that the BSS+ELM WD system formed as a result of Case-A/Case-B MT. In addition to that, one of these eight BSS includes BSS6, which has been previously identified as a likely eclipsing binary (Mazur et al. 1999) and, therefore, would have formed via the Case-A/Case-B formation mechanism. Using Swift/UVOT observations, Rao et al. (2022) found a single BSS out of 11 BSS to be a binary BSS with a hot companion based on the NUV excess. Since UVOT data are in the NUV filters, the detection of unresolved hot companions in Rao et al. (2022) and our work are smaller compared to those found in the FUV-based AstroSat/UVIT observations such as Vaidya et al. (2022); Panthi & Vaidya (2024). This is expected since the excess due to hot WD companions is significant at wavelengths smaller than $\sim 1800 \text{ \AA}$. Therefore the number of BSS with unresolved hot companions in our work represents only a lower limit on the actual numbers of such BSS in this cluster.

Table 2. For each BSS candidate and YSS candidate, *Gaia* source ID in column 2, coordinates in columns 3 and 4, *Swift*/UVOT UVW2, UVM2, and UVW1 fluxes and their associated errors are in columns 5, 6, and 7, respectively.

Name	GAIA DR3 source_id	RA (deg)	DEC (deg)	UV flux (ergs s ⁻¹ cm ⁻² Å ⁻¹)		
				UVW2±err	UVM2±err	UVW1±err
BSS1	3056682289893334912	116.61005	-4.66228	2.40e-17±3.06e-18	2.09e-17±3.27e-18	8.13e-17±5.13e-18
BSS2	3056682083734884736	116.66626	-4.66237	1.13e-16±6.21e-18	9.94e-17±6.92e-18	1.69e-16±6.72e-18
BSS3	3056682874008981888	116.68007	-4.62433	5.39e-17±4.36e-18	6.23e-17±5.48e-18	1.02e-16±5.496e-18
BSS4	3056679060077913088	116.68629	-4.68343	6.41e-16±1.46e-17	4.64e-16±1.47e-17	7.02e-16±1.32e-17
BSS5	3056678750840279296	116.69946	-4.71175	3.71e-16±1.12e-17	3.24e-16±1.23e-17	5.53e-16±1.17e-17
BSS6	3056682702210133632	116.70154	-4.62616	3.93e-17±3.81e-18	3.38e-17±4.07e-18	8.49e-17±5.19e-18
BSS7	3056679472394757504	116.70512	-4.67469	1.54e-16±7.24e-18	1.42e-16±8.21e-18	3.56e-16±9.49e-18
BSS8	3056679231876595584	116.70588	-4.68348	9.79e-17±5.81e-18	1.06e-16±7.09e-18	2.39e-16±7.99e-18
BSS9	3056679266236321024	116.71739	-4.67424	3.09e-17±3.39e-18	2.04e-17±3.31e-18	8.58e-17±5.21e-18
BSS10	3056684214038601344	116.72419	-4.60423	4.09e-16±1.17e-17	3.27e-16±1.23e-17	5.43e-16±1.15e-17
BSS11	3056679369315529728	116.73059	-4.67562	4.90e-16± 1.28e-17	4.42e-16±1.44e-17	7.45e-16±1.35e-17
BSS12	3056679609833686400	116.73173	-4.65667	4.15e-16±1.18e-17	3.89e-16±1.35e-17	5.79e-16±1.19e-17
BSS13	3056684248398335616	116.73739	-4.59998	7.30e-17±5.07e-18	8.54e-17±6.39e-18	1.33e-16±6.09e-18
BSS14	3056678441602599296	116.74244	-4.69012	9.83e-16±1.81e-17	7.79e-16±1.91e-17	6.96e-16±1.31e-17
BSS15	3056681121662156672	116.74742	-4.63435	1.14e-16±6.26e-18	8.78e-17±6.47e-18	1.82e-16±7.03e-18
BSS16	3056678372883126528	116.75689	-4.70461	2.28e-17±2.94e-18	2.16e-17±3.32e-18	5.34e-17±4.54e-18
YSS1	3056679094437661056	116.66802	-4.68711	1.41e-17±2.45e-18	1.1e-17±2.46e-18	1.01e-16±5.69e-18
YSS2	3056679644193433344	116.70590	-4.65552	.03E-17±4.99E-18	6.28e-17±5.52e-18	2.12e-16±7.46e-18

5. ACKNOWLEDGEMENTS

The authors would like to thank Manan Agarwal for developing the ML-MOC algorithm, using which the cluster membership has been determined for this work. This work has made use of the third data release from the European Space Agency (ESA) mission *Gaia* (<https://www.cosmos.esa.int/gaia>), *Gaia* DR3 (Vallenari et al. 2023), processed by the *Gaia* Data Processing and Analysis Consortium (DPAC, <https://www.cosmos.esa.int/web/gaia/dpac/consortium>). This research made use of ASTROPY, a PYTHON package for astronomy (Astropy Collaboration et al. 2013), NUMPY Harris et al. (2020), MATPLOTLIB Hunter & Dale (2007). This research also made use of the Astrophysics Data System (ADS) governed by NASA (<https://ui.adsabs.harvard.edu>).

6. DATA AVAILABILITY

The data underlying this article are publicly available at <https://gea.esac.esa.int/archive>. The derived data generated in this research will be shared upon reasonable request to the corresponding author.

REFERENCES

- Agarwal, M., Rao, K. K., Vaidya, K., & Bhattacharya, S. 2021, Monthly Notices of the Royal Astronomical Society, 502, 2582
- Agrawal, P. C. 2017, Journal of Astrophysics and Astronomy, 38, 27

Table 3. The estimated parameters of the BSS candidates and YSS candidates using best-fitted SEDs. The dashed line in the column 2 represents the value of fractional residual less than 0.01.

Name	Fractional residual in UV			Component	$\log g$	χ_r^2	vgf_b	Temperature	Radius	Luminosity
	UVW2	UVM2	UVW1							
BSS1	0.23	0.09	0.10	single	3.0	117.39	1.53	6500±125	1.05±0.11	1.77±0.35
BSS2	0.23	0.05	–	single	3.0	67.93	1.01	7250±125	1.14±0.11	3.21±0.63
BSS3	0.01	0.02	–	single	4.0	58.04	1.96	6750±125	1.29±0.13	3.12±0.62
BSS4	0.07	–	–	single	3.0	119.61	0.34	8500±125	1.26±0.12	7.46±0.15
BSS5	0.30	0.13	–	single	3.0	33.55	0.21	7250±125	1.96±0.19	9.56±0.18
BSS6	0.22	–	–	single	3.0	78.16	1.71	6750±125	1.06±0.10	2.08±0.41
BSS7	–	–	–	single	3.0	87.05	0.35	7000±125	1.93±0.19	8.09±0.16
BSS8	0.13	0.07	–	single	4.0	122.92	0.77	6750±125	1.63±0.16	5.02±1.01
BSS9	0.32	–	0.03	single	3.0	176.89	1.12	6500±125	1.12±0.11	2.01±0.39
BSS10	0.17	–	–	single	3.0	332.71	0.83	7750±125	1.54±0.15	7.67±1.51
BSS11	0.08	–	–	single	3.0	25.68	1.38	7500±125	2.13±0.21	12.89±2.53
BSS12	0.07	–	–	single	3.0	148.62	0.81	7750±125	1.64±0.16	8.75±1.71
BSS13	0.31	0.34	–	single	3.0	76.93	0.29	7000±125	1.08±0.10	2.51±0.49
BSS14	0.87	0.83	0.64	single	3.0	58.76	3.51	7500±125	1.11±0.11	3.46±0.68
BSS15	0.18	–	–	single	3.0	131.60	0.68	7200±125	1.17±0.12	3.43±0.68
BSS16	0.31	0.34	–	single	3.0	49.02	2.33	6250±125	1.24±0.12	2.12±0.42
	–	–	–	double	3.0	45.28	4.14	12500 ⁺²⁵⁰ _{–500}	0.05±0.01	0.06±0.02
YSS1	–	0.05	–	single	4.0	45.19	0.31	5750±125	2.66±0.21	7.03±1.12
YSS2	0.06	0.03	–	single	3.5	215.68	0.26	6250±125	3.03±0.24	12.91±2.07

- Ahumada, J., & Lapasset, E. 2007, *Astronomy & Astrophysics*, 463, 789
- Althaus, L. G., Bertolami, M. M. M., & Córscico, A. H. 2013, *Astronomy & Astrophysics*, 557, A19
- Astropy Collaboration, Robitaille, T. P., Tollerud, E. J., et al. 2013, *A&A*, 558, A33
- Bailer-Jones, C., Rybizki, J., Fouesneau, M., Demleitner, M., & Andrae, R. 2021, *VizieR Online Data Catalog*, 1352, I
- Bailyn, C. D. 1995, *Annual Review of Astronomy and Astrophysics*, 33, 133
- Boffin, H. M., Carraro, G., Beccari, G., et al. 2015, *Ecology of Blue Straggler Stars*, Vol. 413 (Springer)
- Bragaglia, A., Gratton, R., Carretta, E., et al. 2012, *Astronomy & Astrophysics*, 548, A122
- Bressan, A., Marigo, P., Girardi, L., et al. 2012, *Monthly Notices of the Royal Astronomical Society*, 427, 127
- Brown, J. M., Kilic, M., Brown, W. R., & Kenyon, S. J. 2011, *The Astrophysical Journal*, 730, 67
- Carney, B. W., Latham, D. W., & Laird, J. B. 2005, *The Astronomical Journal*, 129, 466
- Castelli, F., Gratton, R., & Kurucz, R. 1997, *Astronomy and Astrophysics*, v. 318, p. 841-869, 318, 841
- Chand, K., Kunwar Rao, K., Vaidya, K., & Panthi, A. 2024, *Bulletin de la Societe Royale des Sciences de Liege*, 93, 262
- Chen, X., & Han, Z. 2008, *MNRAS*, 387, 1416
- Cohen, M., Wheaton, W. A., & Megeath, S. 2003, *The Astronomical Journal*, 126, 1090
- Cover, T., & Hart, P. 1967, *IEEE transactions on information theory*, 13, 21
- Davies, M. B., Piotto, G., & Angeli, F. D. 2004, *Monthly Notices of the Royal Astronomical Society*, 349, 129
- Dempsey, R. C., Linsky, J. L., Fleming, T. A., & Schmitt, J. 1993, *Astrophysical Journal Supplement Series (ISSN 0067-0049)*, vol. 86, no. 2, p. 599-609., 86, 599
- Fazio, G., Hora, J., Allen, L., et al. 2004, *The Astrophysical Journal Supplement Series*, 154, 10
- Ferraro, F. R., & Lanzoni, B. 2006, *Proceedings of the International Astronomical Union*, 2, 438
- Ferraro, F. R., Lanzoni, B., Dalessandro, E., et al. 2012, *Nature*, 492, 393
- Fiorentino, G., Lanzoni, B., Dalessandro, E., et al. 2014, *The Astrophysical Journal*, 783, 34
- Fitzpatrick, E. L. 1999, *Publications of the Astronomical Society of the Pacific*, 111, 63
- Gaia Collaboration, Brown, A. G. A., & et al. 2021, *Astronomy & Astrophysics*, 649, A1
- Gaia Collaboration, Brown, A. G. A., Vallenari, A., et al. 2018, *Astronomy & Astrophysics*, 616, A1

- Gehrels, N., Chincarini, G., Giommi, P., et al. 2004, *The Astrophysical Journal*, 611, 1005
- Geller, A. M., & Mathieu, R. D. 2011, *Nature*, 478, 356
- Geller, A. M., Leiner, E. M., Bellini, A., et al. 2017, *The Astrophysical Journal*, 840, 66
- Gilliland, R. L., Bono, G., Edmonds, P. D., et al. 1998, *The Astrophysical Journal*, 507, 818
- Gosnell, N. M., Mathieu, R. D., Geller, A. M., et al. 2014, *The Astrophysical Journal Letters*, 783, L8
- Gosnell, N. M., Mathieu, R. D., Geller, A. M., et al. 2015, *ApJ*, 814, 163
- Harris, C. R., Millman, K. J., Van Der Walt, S. J., et al. 2020, *Nature*, 585, 357
- Hills, J., & Day, C. 1976, *Astrophysical Letters*, Vol. 17, p. 87, 17, 87
- Hunter, J., & Dale, D. 2007, *Matplotlib 0.90.0 user's guide*
- Indebetouw, R., Mathis, J., Babler, B., et al. 2005, *The Astrophysical Journal*, 619, 931
- Jadhav, V. V., Pennock, C. M., Subramaniam, A., Sagar, R., & Nayak, P. K. 2021, *MNRAS*, 503, 236
- Jadhav, V. V., Sindhu, N., & Subramaniam, A. 2019, *The Astrophysical Journal*, 886, 13
- Janes, K., & Smith, G. 1984, *Astronomical Journal (ISSN 0004-6256)*, vol. 89, April 1984, p. 487-495., 89, 487
- Jordi, C., Gebran, M., Carrasco, J., et al. 2010, *Astronomy & Astrophysics*, 523, A48
- Kassis, M., Janes, K. A., Friel, E. D., & Phelps, R. L. 1997, *Astronomical Journal* v. 113, p. 1723-1732 (1997), 113, 1723
- Koester, D. 2010, *Memorie della Societa Astronomica Italiana*, 81, 921
- Kouzuma, S. 2019, *Publications of the Astronomical Society of Japan*, 71, 21
- Landsman, W., Aparicio, J., Bergeron, P., Di Stefano, R., & Stecher, T. 1997, *The Astrophysical Journal*, 481, L93
- Leiner, E., Mathieu, R. D., Stello, D., Vanderburg, A., & Sandquist, E. 2016, *The Astrophysical Journal Letters*, 832, L13
- Leiner, E. M., & Geller, A. 2021, *The Astrophysical Journal*, 908, 229
- Leonard, P. J. 1996, *Astrophysical Journal* v. 470, p. 521, 470, 521
- Martin, D. C., Fanson, J., Schiminovich, D., et al. 2005, *The Astrophysical Journal*, 619, L1
- Mathieu, R., Geller, A., Gosnell, N., & Szentgyorgyi, A. 2009, *NOAO Proposal*, 328
- Mathieu, R. D., Latham, D. W., & Griffin, R. 1990, *Astronomical Journal (ISSN 0004-6256)*, vol. 100, Dec. 1990, p. 1859-1881., 100, 1859
- Mazur, B., Krzeminski, W., & Kaluzny, J. 1999, *Acta Astronomica*, v. 49, pp. 551-560,(1999)., 49, 551
- Mitra-Kraev, U., Harra, L. K., Güdel, M., et al. 2005, *Astronomy & Astrophysics*, 431, 679
- Momany, Y., Held, E., Saviane, I., et al. 2007, *Astronomy & Astrophysics*, 468, 973
- Nikitha, K., Vig, S., & Ghosh, S. 2022, *Monthly Notices of the Royal Astronomical Society*, 514, 5570
- Panei, J. A., Althaus, L. G., Chen, X., & Han, Z. 2007, *Monthly Notices of the Royal Astronomical Society*, 382, 779
- Panthi, A., & Vaidya, K. 2024, *Monthly Notices of the Royal Astronomical Society*, 527, 10335
- Panthi, A., Vaidya, K., Jadhav, V., et al. 2022, *Monthly Notices of the Royal Astronomical Society*, 516, 5318
- Panthi, A., Vaidya, K., Vernekar, N., et al. 2024, *Monthly Notices of the Royal Astronomical Society*, 527, 8325
- Peel, D., & McLachlan, G. J. 2000, *Statistics and computing*, 10, 339
- Perets, H. B., & Fabrycky, D. C. 2009, *The Astrophysical Journal*, 697, 1048
- Rain, M., Ahumada, J., & Carraro, G. 2021, *Astronomy & Astrophysics*, 650, A67
- Rao, K. K., Vaidya, K., Agarwal, M., Balan, S., & Bhattacharya, S. 2023, *Monthly Notices of the Royal Astronomical Society*, 526, 1057
- Rao, K. K., Vaidya, K., Agarwal, M., & Bhattacharya, S. 2021, *Monthly Notices of the Royal Astronomical Society*, 508, 4919
- Rao, K. K., Vaidya, K., Agarwal, M., et al. 2022, *Monthly Notices of the Royal Astronomical Society*, 516, 2444
- Ritter, H. 2010, *Memorie della Societa Astronomica Italiana*, v. 81, p. 849 (2010), 81, 849
- Roming, P. W., Kennedy, T. E., Mason, K. O., et al. 2005, *Space Science Reviews*, 120, 95
- Saketh, P., Panthi, A., & Vaidya, K. 2024, *The Astronomical Journal*, 168, 97
- Sandage, A. 1953, *Astronomical Journal*, Vol. 58, p. 61-75 (1953), 58, 61
- Schlafly, E., Finkbeiner, D., Jurić, M., et al. 2012, *The Astrophysical Journal*, 756, 158
- Shara, M. M., Saffer, R. A., & Livio, M. 1997, *The Astrophysical Journal*, 489, L59
- Siegel, M., Laporte, S., Porterfield, B., Hagen, L., & Gronwall, C. 2019, *VizieR Online Data Catalog*, J
- Sindhu, N., Subramaniam, A., Jadhav, V. V., et al. 2019, *The Astrophysical Journal*, 882, 43
- Strom, S. E., Strom, K. M., & Bregman, J. N. 1971, *Publications of the Astronomical Society of the Pacific*, 83, 768

- Subramaniam, A., Sindhu, N., Tandon, S., et al. 2016, *The Astrophysical Journal Letters*, 833, L27
- Subramaniam, A., et al. 2018, *Monthly Notices of the Royal Astronomical Society*, 481, 226
- Tonry, J., Stubbs, C. W., Lykke, K. R., et al. 2012, *The Astrophysical Journal*, 750, 99
- Vaidya, K., Panthi, A., Agarwal, M., et al. 2022, *Monthly Notices of the Royal Astronomical Society*, 511, 2274
- Vaidya, K., Rao, K. K., Agarwal, M., & Bhattacharya, S. 2020, *Monthly Notices of the Royal Astronomical Society*, 496, 2402
- Vallenari, A., Brown, A. G., Prusti, T., et al. 2023, *Astronomy & Astrophysics*, 674, A1
- Vilhu, O. 1982, *Astronomy and Astrophysics*, vol. 109, no. 1, May 1982, p. 17-22., 109, 17
- Wang, S., & Chen, X. 2019, *The Astrophysical Journal*, 877, 116
- Wright, E. L., Eisenhardt, P. R., Mainzer, A. K., et al. 2010, *The Astronomical Journal*, 140, 1868